

# Supporting information

## Magneto-structural correlation in lanthanide luminescent [2.2]Paracyclophane-based Single-Molecule Magnets

Hadrien Flichot,<sup>1</sup> Annika Sickinger,<sup>2</sup> Jules Brom,<sup>3</sup> Bertrand Lefeuvre,<sup>1</sup> Vincent Dorcet,<sup>1</sup> Thierry Guizouarn,<sup>1</sup> Olivier Cador,<sup>1</sup> Boris Le Guennic,<sup>1</sup> Laurent Micouin,<sup>3</sup> Olivier Maury,<sup>2</sup> Erica Benedetti,<sup>\*3</sup> Fabrice Pointillart<sup>\*1</sup>

<sup>1</sup> *Univ Rennes, CNRS, ISCR (Institut des Sciences Chimiques de Rennes) – UMR 6226, 35000 Rennes (France)*

*E-mail: fabrice.pointillart@univ-rennes1.fr*

<sup>2</sup> *Univ Lyon, ENS de Lyon, Université Claude Bernard Lyon 1, CNRS UMR 5182, Laboratoire de Chimie, Lyon F-69342, France*

<sup>3</sup> *Université Paris Cité, CNRS, Laboratoire de Chimie et de Biochimie Pharmacologiques et Toxicologiques, F-75006 Paris, France*

*E-mail: erica.benedetti@u-paris.fr*

**Table S1.** Summary of X-ray crystallographic data for compounds **1-5**.

Compound	[Dy(hfac) <sub>3</sub> (L)] ( <b>1-Dy</b> )	[Yb(hfac) <sub>3</sub> (L)] ( <b>2-Yb</b> )	[Dy(tta) <sub>3</sub> (L)] ( <b>3-Dy</b> )
Formula	C <sub>55</sub> H <sub>37</sub> DyF <sub>18</sub> O <sub>8</sub> P <sub>2</sub>	C <sub>55</sub> H <sub>37</sub> F <sub>18</sub> O <sub>8</sub> P <sub>2</sub> Yb	C <sub>64</sub> H <sub>46</sub> DyF <sub>9</sub> O <sub>8</sub> P <sub>2</sub> S <sub>3</sub>
M / g.mol <sup>-1</sup>	1392.28	1439.86	1434.63
Crystal system	monoclinic	tetragonal	monoclinic
Space group	P2 <sub>1</sub> /n	I4 <sub>1</sub> /acd	P2 <sub>1</sub> /n
Cell parameters	a=14.0066(11) Å b=19.4597(17) Å c=20.4412(18) Å α=90° β=92.335(3)° γ=90°	a=29.5507(6) Å b=29.5507 Å c=26.1095(6) Å α=90° β=90° γ=90°	a=14.6220(15) Å b=19.582(2) Å c=20.966(3) Å α=90° β=101.049(4)° γ=90°
Volume / Å <sup>3</sup>	5566.9(8)	22800.0(11)	5892.0(12)
Z	4	16	4
T / K	150(2)	150(2)	150(2)
θ range /°	2.2522 ≤ θ ≤ 27.4835	2.6047 ≤ θ ≤ 27.4734	2.8037 ≤ θ ≤ 26.1439
ρ <sub>calc</sub> / g.cm <sup>-3</sup>	1.661	1.678	1.617
μ / mm <sup>-1</sup>	1.513	1.810	1.514
Number of reflections	64023	51639	85875
Independent reflections	12726	6534	13556
R <sub>int</sub>	0.0545	0.0401	0.0909
Fo <sup>2</sup> > 2σ(Fo) <sup>2</sup>	11156	5551	10142
Number of variables	749	435	850
R1, ωR2	0.0493, 0.1253	0.0710, 0.1982	0.0560, 0.1096
Compounds	[Yb(tta) <sub>3</sub> (L)] ( <b>4-Yb</b> )	[Na(Dy <sub>2</sub> (hfac) <sub>6</sub> (L) <sub>2</sub> )] [BArF] ( <b>5-Dy</b> )	
Formula	C <sub>64</sub> H <sub>46</sub> F <sub>9</sub> O <sub>8</sub> P <sub>2</sub> S <sub>3</sub> Yb	C <sub>142</sub> H <sub>85</sub> BDy <sub>2</sub> F <sub>60</sub> NaO <sub>16</sub> P <sub>4</sub>	
M / g.mol <sup>-1</sup>	1445.17	3669.77	
Crystal system	monoclinic	Triclinic	
Space group	P2 <sub>1</sub> /n	P-1	
Cell parameters	a=14.6087(10) Å b=19.6278(13) Å c=20.8238(16) Å α=90° β=100.797(3)° γ=90°	a=13.426(5) Å b=21.081(7) Å c=27.045(10) Å α=85.259(10)° β=84.050(10)° γ=78.874(9)°	
Volume / Å <sup>3</sup>	5865.2(7)	7455(5)	
Z	4	2	
T / K	150(2)	150(2)	
θ range /°	2.147 ≤ θ ≤ 27.506	1.862 ≤ θ ≤ 27.984	
ρ <sub>calc</sub> / g.cm <sup>-3</sup>	1.637	1.635	

$\mu / \text{mm}^{-1}$	1.842	1.177	
Number of reflections	45711	161273	
Independent reflections	13400	34446	
$R_{\text{int}}$	0.0441	0.1539	
$F_o^2 > 2\sigma(F_o)^2$	10752	17227	
Number of variables	786	1982	
$R1, \omega R2$	0.0458, 0.1075	0.2031, 0.4421	

**Table S2.** SHAPE analyses for compounds **1-4**.

Compounds	Shape calculations			
	SAPR-8 (D4d)	TDD-8 (D2d)	JBTPR-8 (C2v)	BTPR-8 (C2v)
<b>1-Dy</b>	2.416	0.63	2.566	2.198
<b>2-Yb</b>	1.171	0.962	2.2	1.975
<b>3-Dy</b>	2.671	0.826	1.629	1.336
<b>4-Yb</b>	2.66	0.675	1.673	1.442

\*TDD-8 corresponds to a Triangular dodecahedron geometry, BTPR-8 to a Biaugmented trigonal prism, JBTPR-8 to a Biaugmented trigonal prism J50 and to SAPR-8 to Square antiprism.

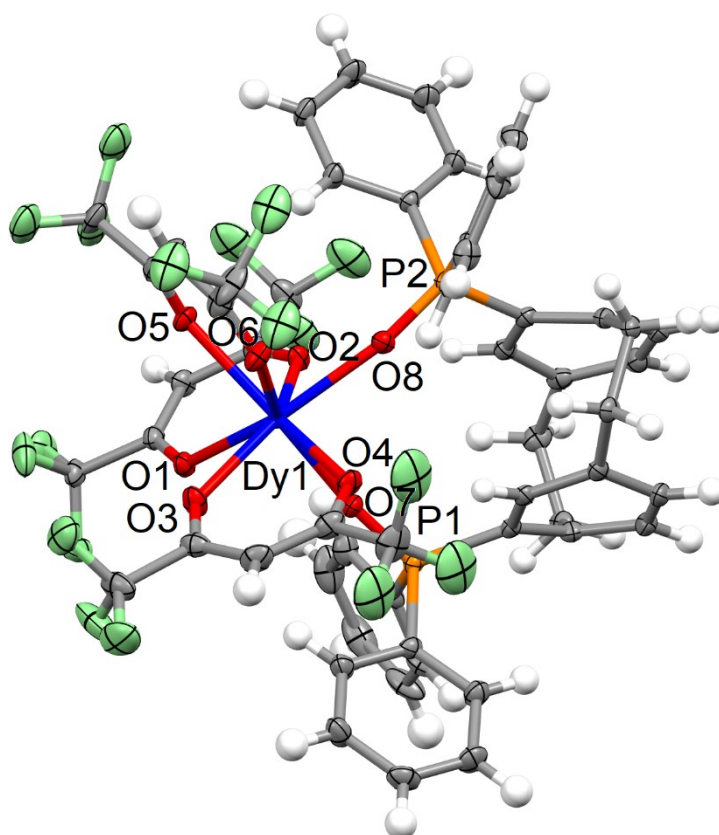


**Figure S1.** Ortep view of the asymmetric unit for **1-Dy**. Thermal ellipsoids are drawn at 30% probability.

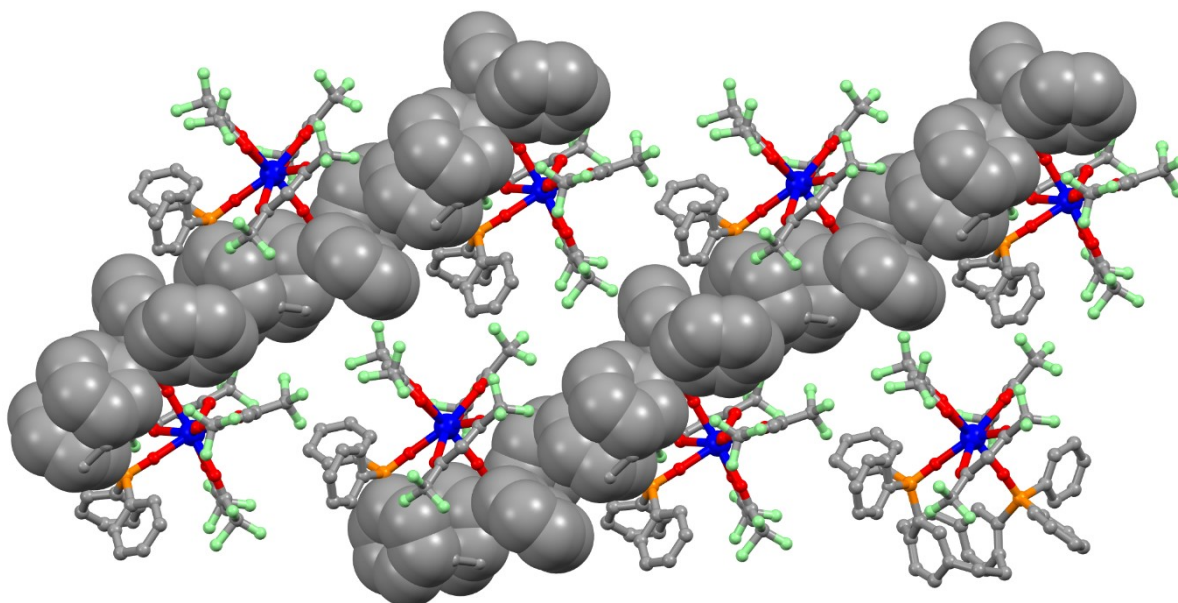


**Figure S2.** Crystal packing of **1-Dy** highlighting the  $\pi$ -interactions between the phenyl rings of the paracyclophane and bisphenyl oxophosphine groups (spacefill representation).

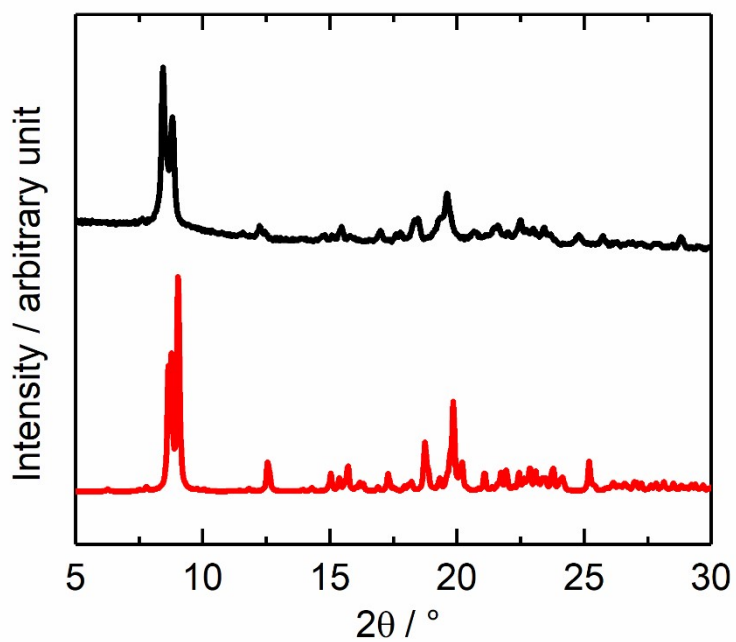


**Figure S3.** Experimental (black line) and simulated (red line) PXRD of **1-Dy**.

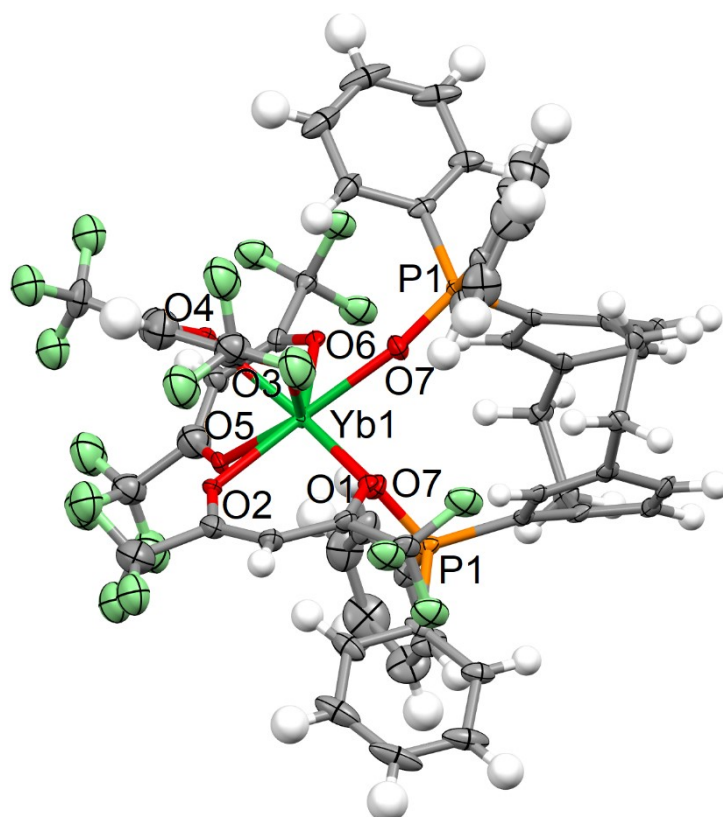


**Figure S4.** Ortep view of the asymmetric unit for **2-Yb**. Thermal ellipsoids are drawn at 30% probability.

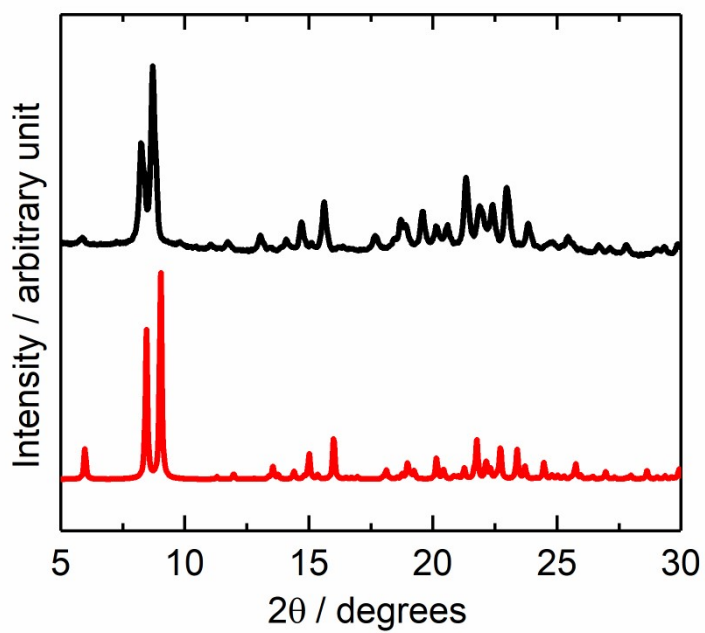


**Figure S5.** Experimental (black line) and simulated (red line) PXRD of **2-Yb**.

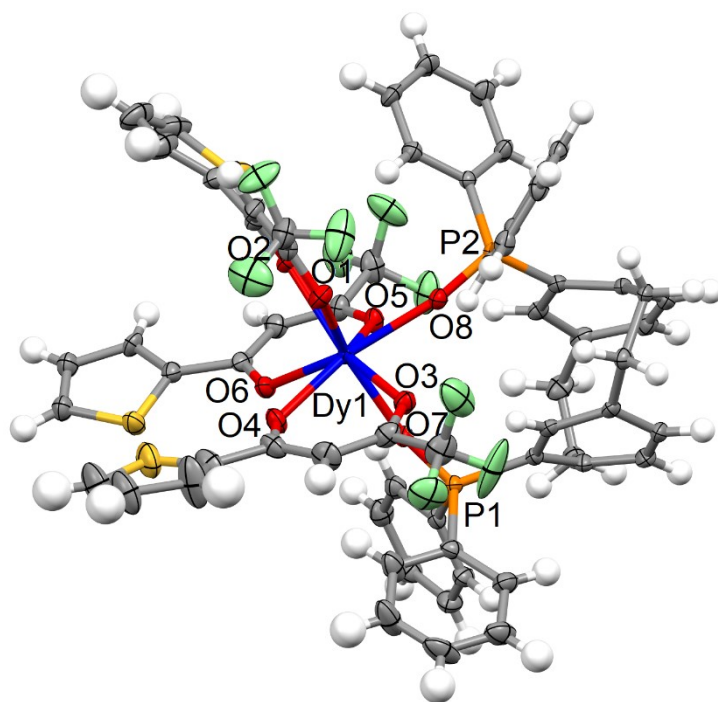


**Figure S6.** Ortep view of the asymmetric unit for **3-Dy**. Thermal ellipsoids are drawn at 30% probability.

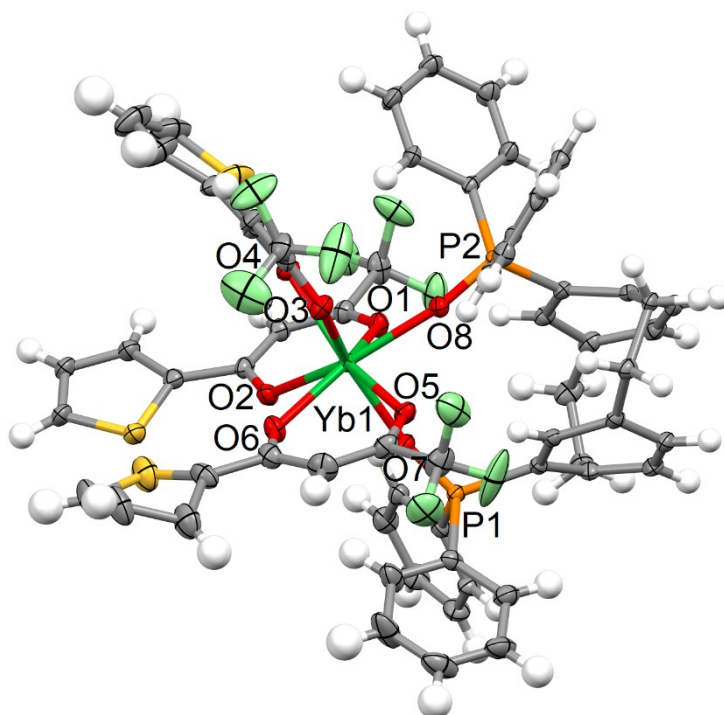


**Figure S7.** Ortep view of the asymmetric unit for **4-Yb**. Thermal ellipsoids are drawn at 30% probability.

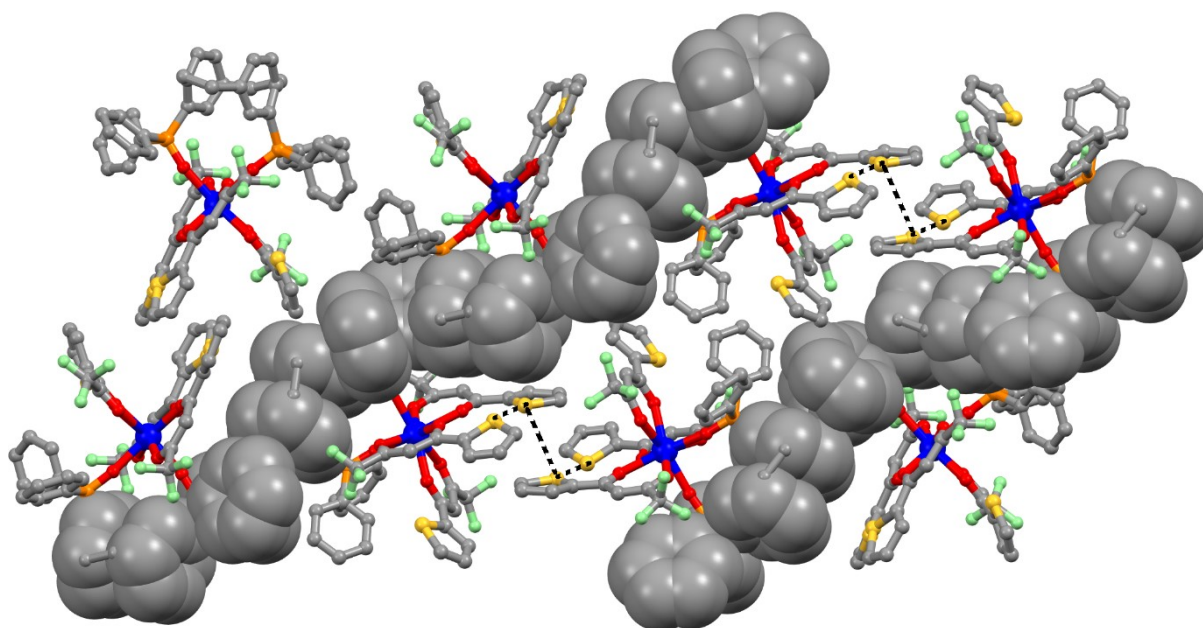


**Figure S8.** Crystal packing of **3-Dy** highlighting the  $\pi$ -interactions between the phenyl rings of the paracyclophane and bisphenyl oxophosphine groups (spacefill representation) as well as intra- and inter-molecular S...S short contacts.

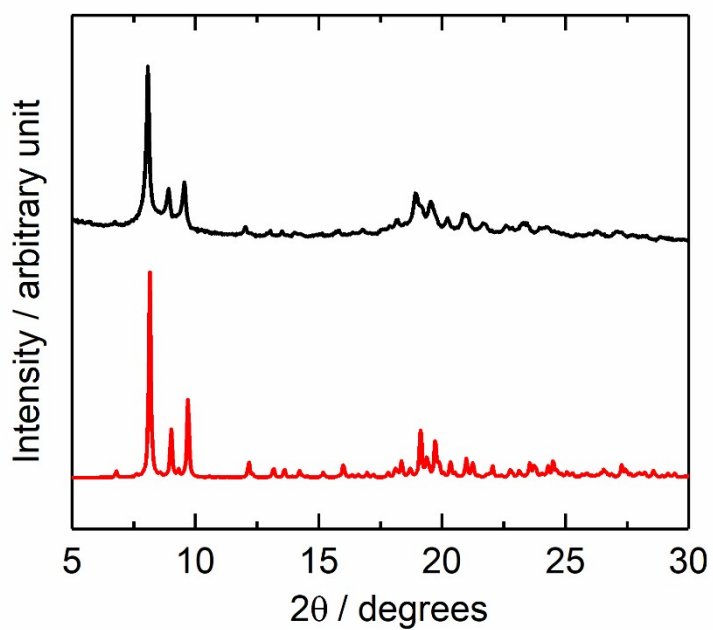


**Figure S9.** Experimental (black line) and simulated (red line) PXRD of **3-Dy**.

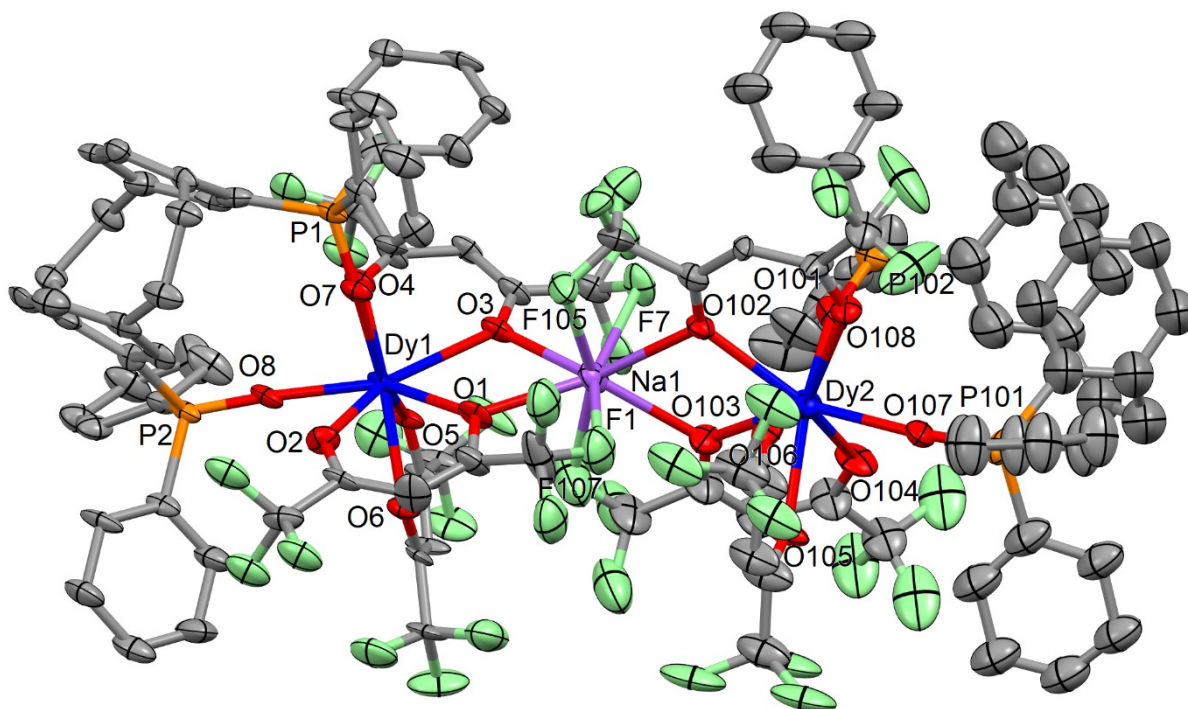


**Figure S10.** Ortep view of the asymmetric unit for **5-Dy**. Thermal ellipsoids are drawn at 30% probability. Hydrogen atoms are omitted for clarity reason. BARF<sup>-</sup> anion is omitted for clarity reason.

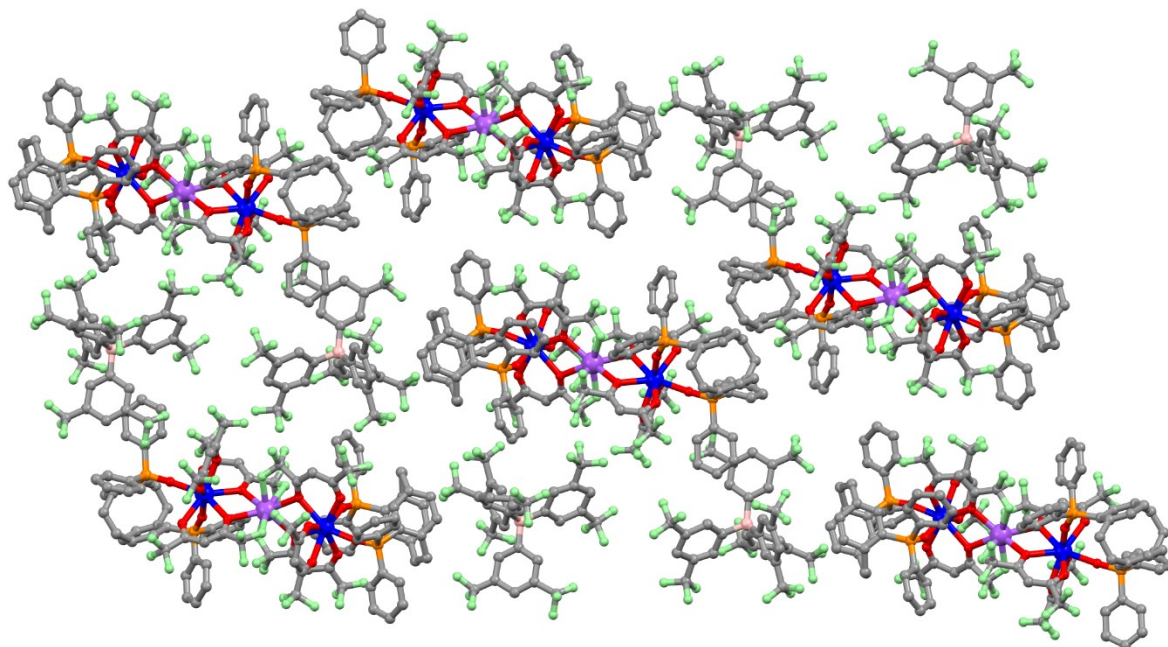


**Figure S11.** Crystal packing of **5-Dy**.

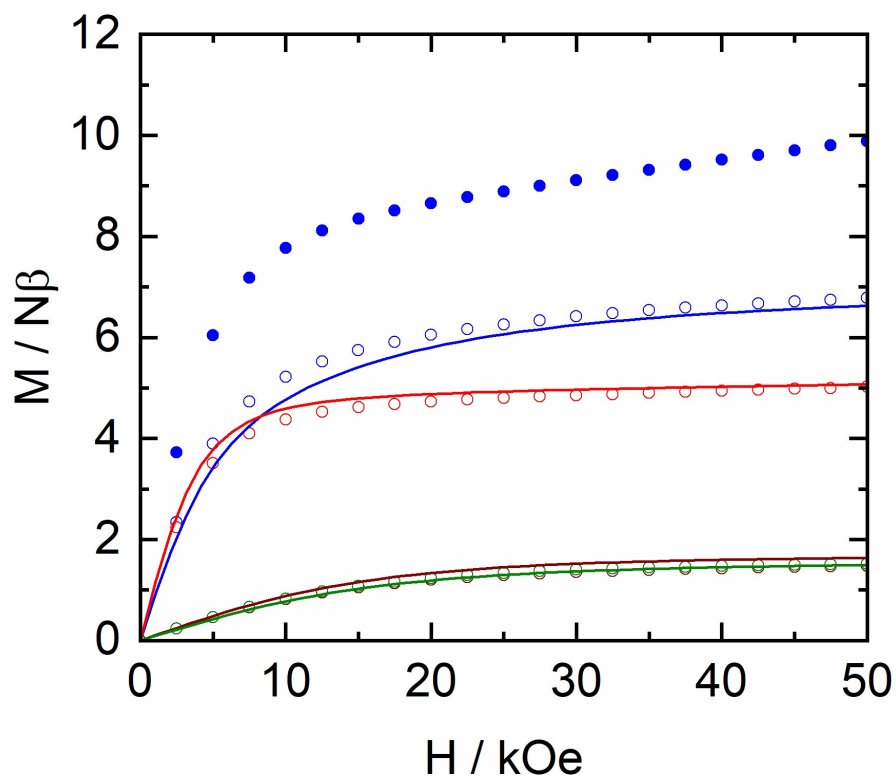


**Figure S12.** Field dependence of the magnetization at 2 K for complexes **1-Dy** (open blue circles), **2-Yb** (open wine circles), **3-Dy** (open red circles), **4-Yb** (open green circles) and **5-Dy** (full blue circles). Full lines correspond to calculated data.

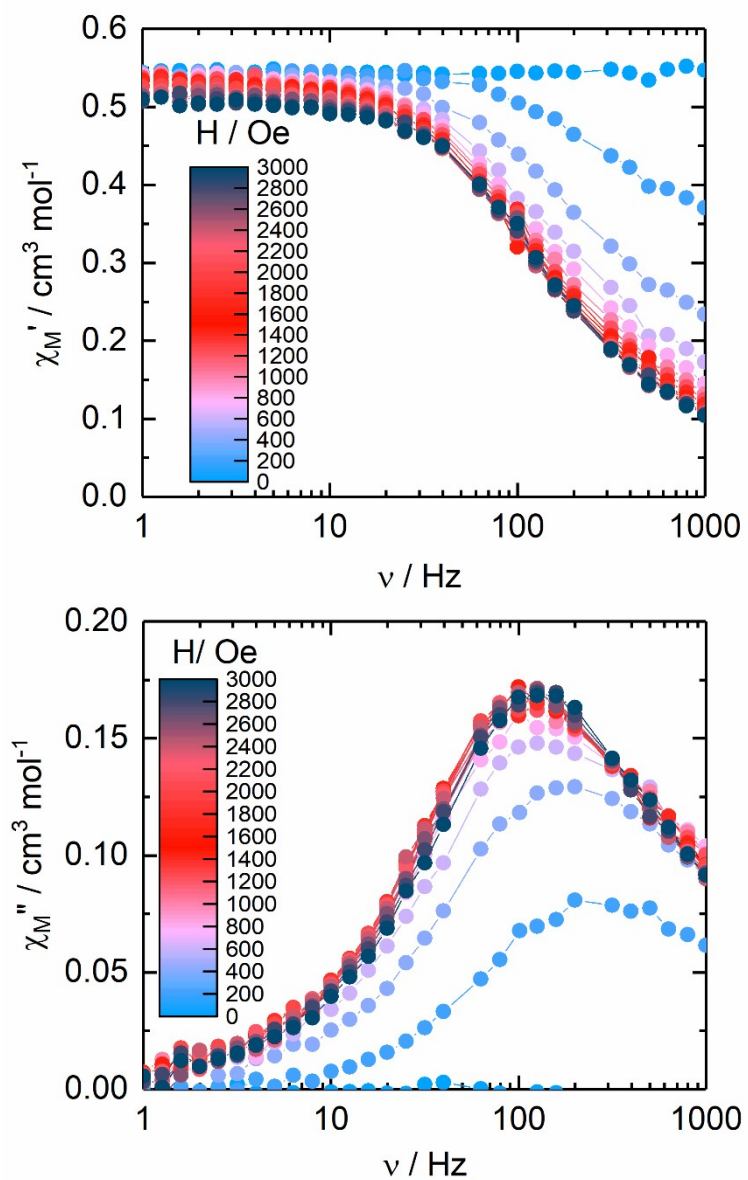


**Figure S13.** Field dependence of the in-phase (top) and out-of-phase (bottom) components of the magnetic susceptibility for **2-Yb** at 2 K in the 0-3000 Oe field range.

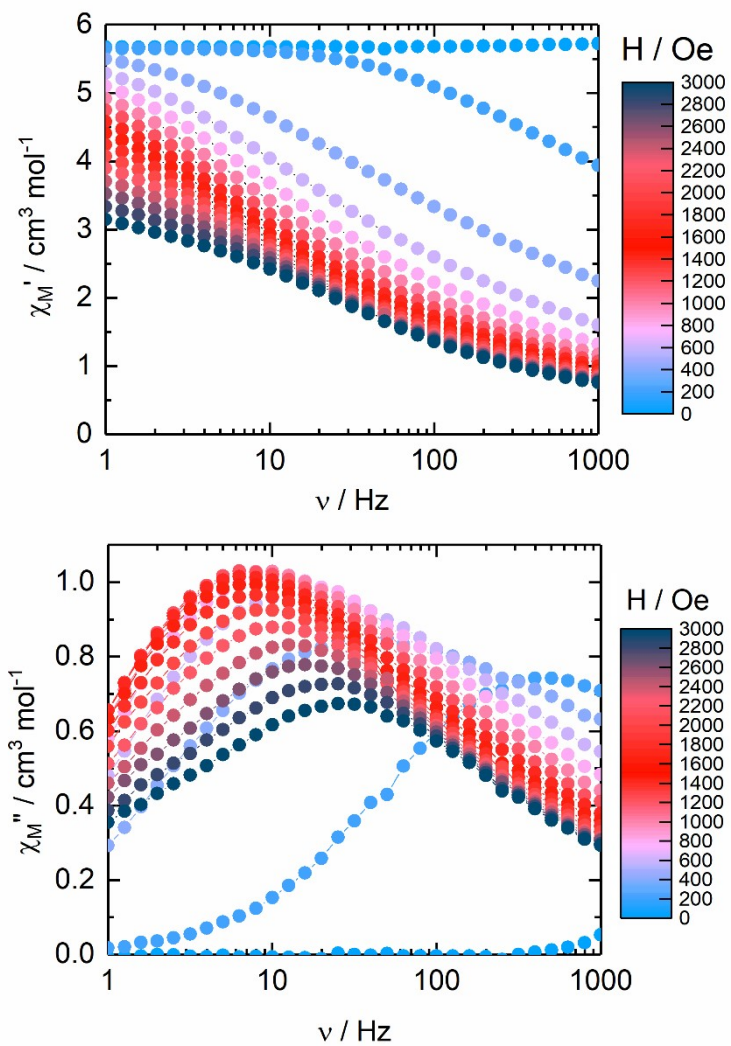


**Figure S14.** Field dependence of the in-phase (top) and out-of-phase (bottom) components of the magnetic susceptibility for **3-Dy** at 2 K in the 0-3000 Oe field range.

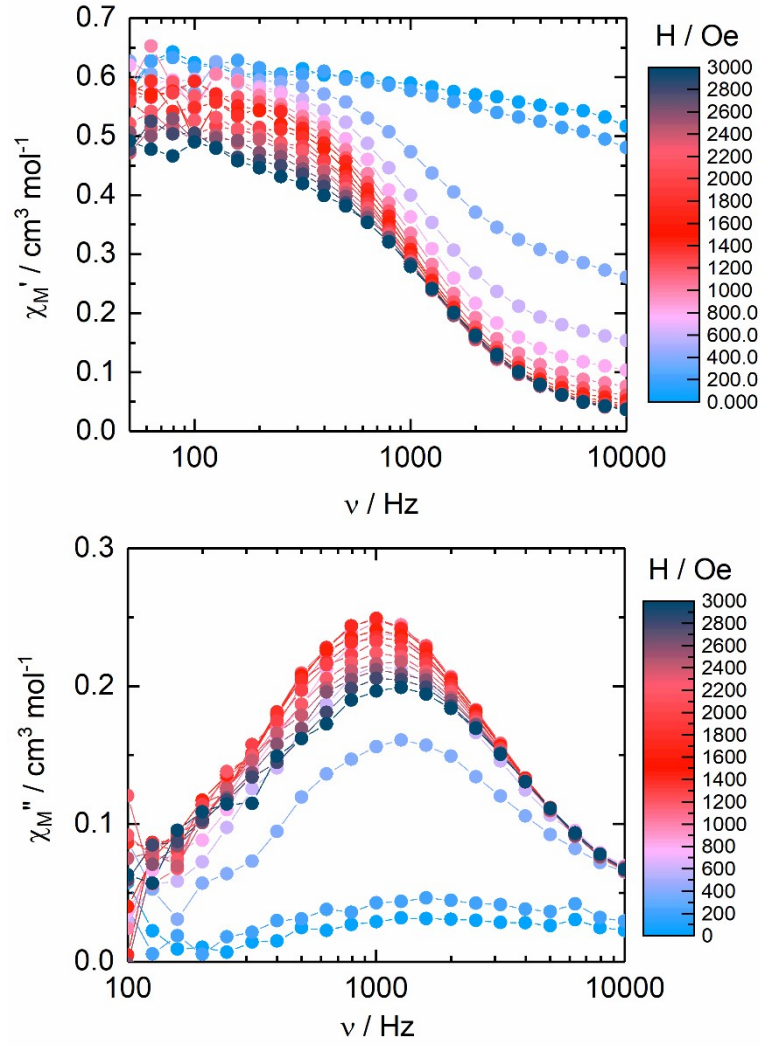


**Figure S15.** Field dependence of the in-phase (top) and out-of-phase (bottom) components of the magnetic susceptibility for **4-Yb** at 2 K in the 0-3000 Oe field range.

**Extended Debye model (Eq. S1).**

$$\chi_M' = \chi_S + (\chi_T - \chi_S) \frac{1 + (\omega\tau)^{1-\alpha} \sin\left(\alpha \frac{\pi}{2}\right)}{1 + 2(\omega\tau)^{1-\alpha} \sin\left(\alpha \frac{\pi}{2}\right) + (\omega\tau)^{2-2\alpha}}$$

$$\chi_M'' = (\chi_T - \chi_S) \frac{(\omega\tau)^{1-\alpha} \cos\left(\alpha \frac{\pi}{2}\right)}{1 + 2(\omega\tau)^{1-\alpha} \sin\left(\alpha \frac{\pi}{2}\right) + (\omega\tau)^{2-2\alpha}}$$

With  $\chi_T$  the isothermal susceptibility,  $\chi_S$  the adiabatic susceptibility,  $\tau$  the relaxation time and  $\alpha$  an empiric parameter which describe the distribution of the relaxation time. For SMM with only one relaxation time,  $\alpha$  is close to zero. The extended Debye model was applied to fit

simultaneously the experimental variations of  $\chi_M'$  and  $\chi_M''$  with the frequency  $\nu$  of the oscillating field ( $\omega = 2\pi\nu$ ). Typically, only the temperatures for which a maximum on the  $\chi''$  vs.  $\nu$  curves, have been considered. The best fitted parameters  $\tau$ ,  $\alpha$ ,  $\chi_T$ ,  $\chi_S$  are listed in Tables S3-S8 with the coefficient of determination  $R^2$ .

**Table S3.** Best fitted parameters ( $\chi_T$ ,  $\chi_S$ ,  $\tau$  and  $\alpha$ ) with the extended Debye model for compound **2-Yb** at 2 K in the field range 200-3000 Oe.

H / Oe	$\chi_S / \text{cm}^3 \text{mol}^{-1}$	$\chi_T / \text{cm}^3 \text{mol}^{-1}$	$\alpha$	$\tau / \text{s}$	$R^2$
200	0.34019	0.54549	0.13323	5.51137E-4	0.99982
400	0.1805	0.54535	0.19851	7.42747E-4	0.99967
600	0.11059	0.54552	0.22858	8.71185E-4	0.99904
800	0.09181	0.54826	0.22673	9.91181E-4	0.99866
1000	0.07994	0.54562	0.22051	0.00103	0.99908
1200	0.07672	0.54434	0.21722	0.0011	0.99858
1400	0.06962	0.54094	0.21715	0.00109	0.99902
1600	0.07313	0.53922	0.20891	0.00118	0.99848
1800	0.06864	0.53588	0.20551	0.00117	0.99905
2000	0.06391	0.53331	0.20602	0.00114	0.999
2200	0.06548	0.52726	0.19331	0.00117	0.99914
2400	0.06625	0.52367	0.18643	0.00115	0.99896
2600	0.06500	0.52011	0.18399	0.00111	0.99911
2800	0.06875	0.51529	0.17358	0.00111	0.99911
3000	0.06419	0.51118	0.17289	0.00105	0.99941

**Table S4.** Best fitted parameters ( $\chi_T$ ,  $\chi_S$ ,  $\tau$  and  $\alpha$ ) with the extended Debye model for compound **3-Dy** at 2 K in the field range 200-3000 Oe.

H / Oe	$\chi_S / \text{cm}^3 \text{mol}^{-1}$	$\chi_T / \text{cm}^3 \text{mol}^{-1}$	$\alpha$	$\tau / \text{s}$	$R^2$
200	3.14753	5.69988	0.32232	4.11314E-4	0.99992
400	1.36169	6.08265	0.55464	0.003	0.99964
600	0.92756	6.22063	0.55367	0.00752	0.99947
800	0.75556	6.22061	0.54993	0.0115	0.99942
1000	0.67067	6.1394	0.54626	0.01472	0.99942
1200	0.62644	6.00389	0.5409	0.01714	0.99938
1400	0.60513	5.79894	0.53201	0.01839	0.99937
1600	0.59358	5.54337	0.52093	0.01825	0.99936
1800	0.58202	5.25821	0.50918	0.01709	0.99941
2000	0.55855	4.96411	0.50064	0.01519	0.99953
2200	0.54722	4.64498	0.48877	0.01303	0.99968
2400	0.52175	4.34011	0.48324	0.01093	0.99978
2600	0.49395	4.06566	0.48115	0.00927	0.99983
2800	0.4658	3.79643	0.48183	0.00773	0.99988
3000	0.42145	3.54962	0.48934	0.00636	0.99989

**Table S5.** Best fitted parameters ( $\chi_T$ ,  $\chi_S$ ,  $\tau$  and  $\alpha$ ) with the extended Debye model for compound **4-Yb** at 2 K in the field range 400-3000 Oe.

H / Oe	$\chi_S / \text{cm}^3 \text{mol}^{-1}$	$\chi_T / \text{cm}^3 \text{mol}^{-1}$	$\alpha$	$\tau / \text{s}$	$R^2$
400	0.25121	0.61445	0.08071	1.18837E-4	0.99936
600	0.1437	0.59936	0.04077	1.36542E-4	0.99609
800	0.09275	0.60027	0.04188	1.47685E-4	0.99657
1000	0.06218	0.60366	0.06189	1.55846E-4	0.99532
1200	0.04431	0.58911	0.06652	1.56836E-4	0.99542
1400	0.04167	0.57935	0.04843	1.57253E-4	0.99595
1600	0.02871	0.57248	0.07818	1.58032E-4	0.9957
1800	0.02498	0.56085	0.08061	1.5722E-4	0.99939
2000	0.02027	0.54993	0.0887	1.55697E-4	0.99672
2200	0.01611	0.54648	0.10615	1.55593E-4	0.9995
2400	0.0144	0.53496	0.11148	1.52183E-4	0.9997
2600	0.01592	0.51083	0.09567	1.43613E-4	0.99571
2800	0.00846	0.50533	0.12737	1.40811E-4	0.99922
3000	0.00549	0.49453	0.13866	1.365E-4	0.99488

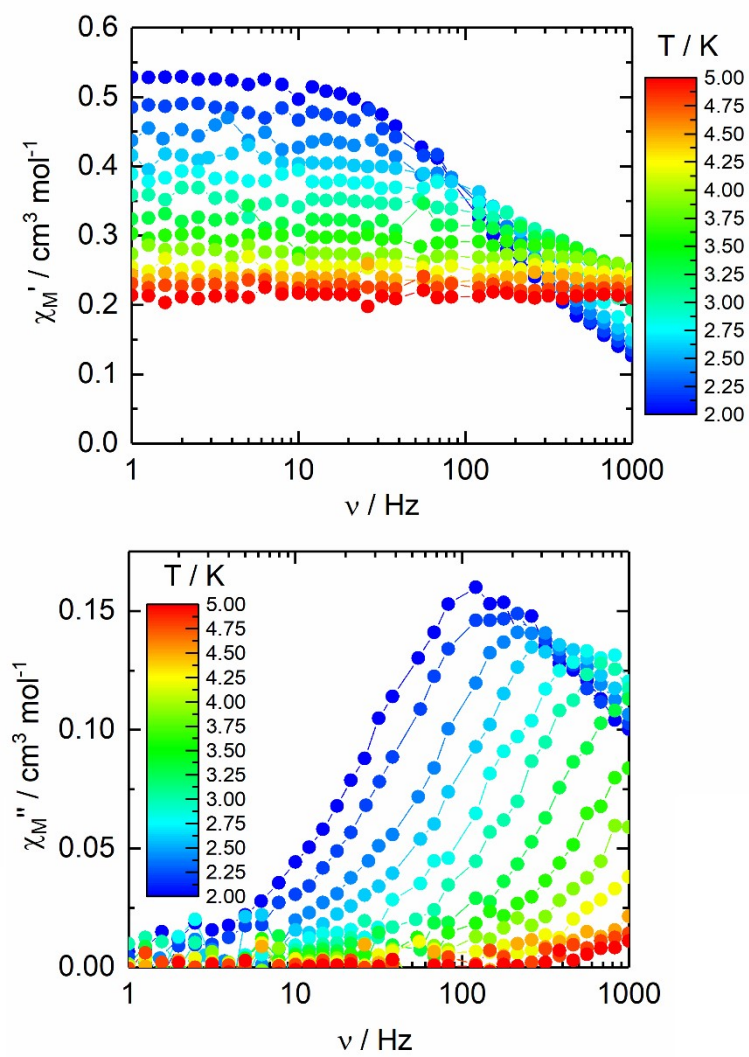


**Figure S16.** Temperature dependence of the in-phase (top) and out-of-phase (bottom) components of the magnetic susceptibility for **2-Yb** at 1000 Oe in the 2-5 K temperature range.

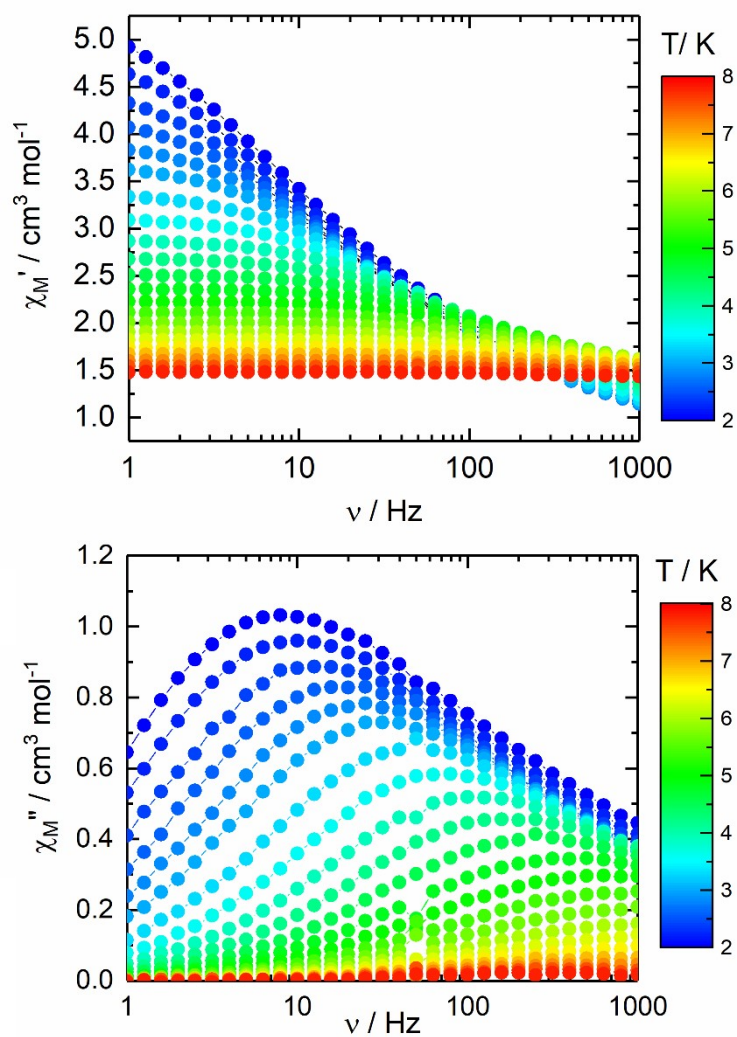


**Figure S17.** Temperature dependence of the in-phase (top) and out-of-phase (bottom) components of the magnetic susceptibility for **3-Dy** at 1000 Oe in the 2-8 K temperature range.

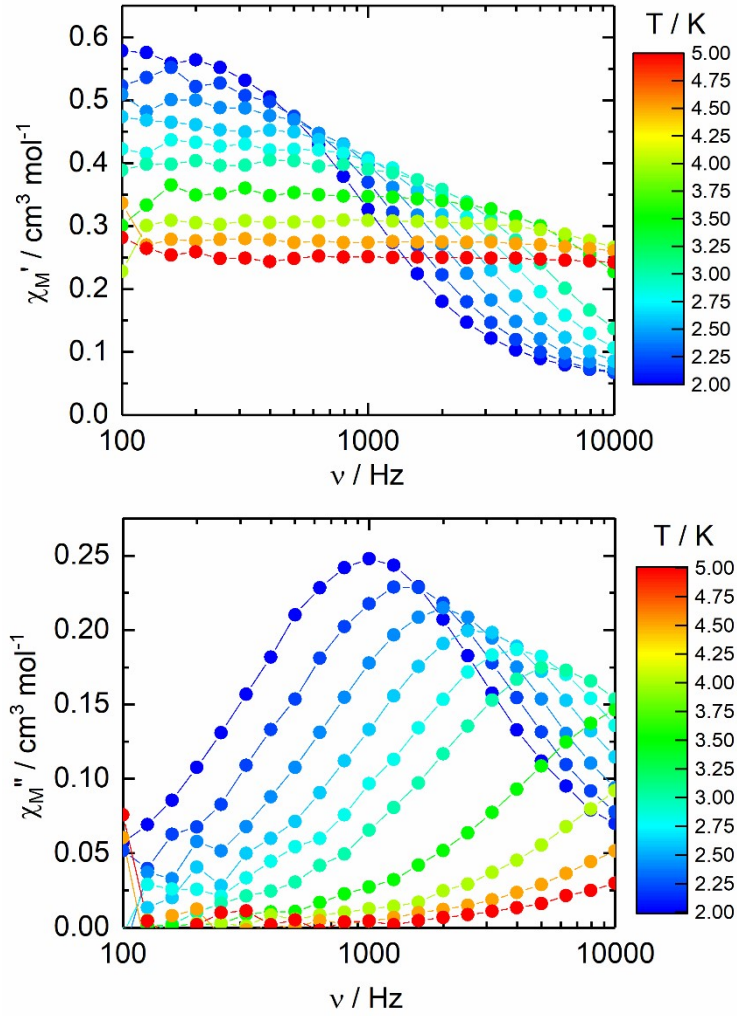


**Figure S18.** Temperature dependence of the in-phase (top) and out-of-phase (bottom) components of the magnetic susceptibility for **4-Yb** at 1000 Oe in the 2-5 K temperature range.

**Table S6.** Best fitted parameters ( $\chi_T$ ,  $\chi_S$ ,  $\tau$  and  $\alpha$ ) with the extended Debye model for compound **2-Yb** at 1000 Oe in the temperature range 2-3.3 K.

T / K	$\chi_S / \text{cm}^3 \text{mol}^{-1}$	$\chi_T / \text{cm}^3 \text{mol}^{-1}$	$\alpha$	$\tau / \text{s}$	$R^2$
2	0.07489	0.52476	0.23203	0.00103	0.99871
2.2	0.08085	0.48155	0.19298	8.12059E-4	0.99867
2.4	0.06668	0.43979	0.19646	5.44126E-4	0.99697
2.6	0.06782	0.40455	0.15018	3.97624E-4	0.99818
2.8	0.05517	0.37585	0.13755	2.68545E-4	0.9987
3	0.04446	0.34626	0.12663	1.7908E-4	0.99753
3.3	0.04265	0.31594	0.09116	1.12776E-4	0.99788

**Table S7.** Best fitted parameters ( $\chi_T$ ,  $\chi_S$ ,  $\tau$  and  $\alpha$ ) with the extended Debye model for compound **3-Dy** at 1000 Oe in the temperature range 2-5.7 K.

T / K	$\chi_S / \text{cm}^3 \text{mol}^{-1}$	$\chi_T / \text{cm}^3 \text{mol}^{-1}$	$\alpha$	$\tau / \text{s}$	$R^2$
2	0.66124	6.18759	0.55092	0.01525	0.99942
2.2	0.72983	5.57466	0.52404	0.01203	0.99931
2.4	0.77758	4.97889	0.49425	0.00877	0.99936
2.6	0.82268	4.53235	0.46429	0.00666	0.99938
2.8	0.84203	4.16685	0.44253	0.00503	0.99941
3	0.86768	3.8613	0.42187	0.00386	0.99952
3.3	0.893	3.48823	0.39954	0.00258	0.99962
3.6	0.92037	3.18934	0.38706	0.00175	0.99973
3.9	0.95715	2.93693	0.37598	0.00119	0.9998
4.2	0.99461	2.72987	0.37276	8.34502E-4	0.99984
4.5	1.05364	2.54299	0.36129	6.01076E-4	0.99991
4.8	1.10705	2.3853	0.36449	4.32505E-4	0.9999
5.1	1.15067	2.2476	0.36851	3.14057E-4	0.99994
5.4	1.20166	2.12715	0.37771	2.43764E-4	0.99988
5.7	1.26923	2.01688	0.37501	2.07291E-4	0.99993

**Table S8.** Best fitted parameters ( $\chi_T$ ,  $\chi_S$ ,  $\tau$  and  $\alpha$ ) with the extended Debye model for compound **4-Yb** at 1000 Oe in the temperature range 2-3 K.

T / K	$\chi_S / \text{cm}^3 \text{mol}^{-1}$	$\chi_T / \text{cm}^3 \text{mol}^{-1}$	$\alpha$	$\tau / \text{s}$	$R^2$
2	0.05178	0.59676	0.0619	1.57138E-4	0.99952
2.2	0.04909	0.54827	0.05301	1.13604E-4	0.99931
2.4	0.04741	0.50276	0.03931	8.05052E-5	0.99949
2.6	0.04513	0.46366	0.02984	5.67316E-5	0.99945
2.8	0.0389	0.43448	0.03802	3.9833E-5	0.9996
3	0.04361	0.4032	0.01613	2.86157E-5	0.99957

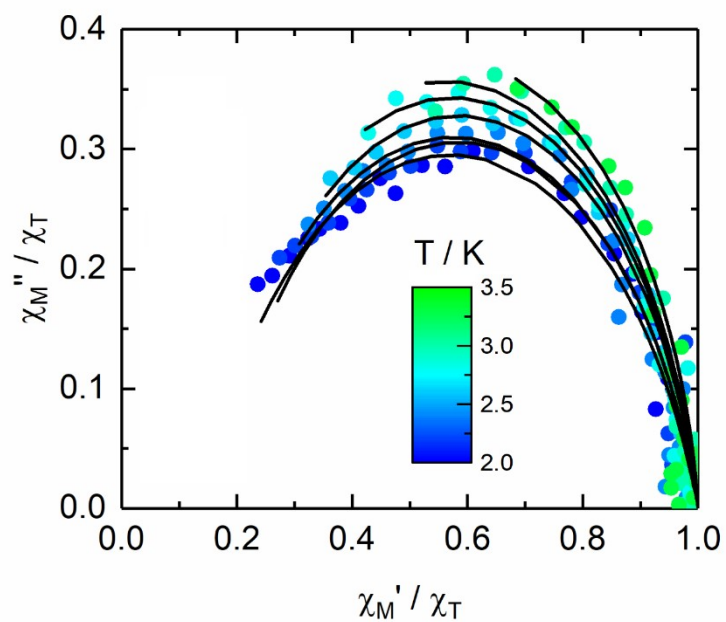


**Figure S19.** Normalized Argand plot for **2-Yb** in the temperature range of 2-3.5 K at 1000 Oe. Full black lines are the best fits obtained from the extended Debye equation.

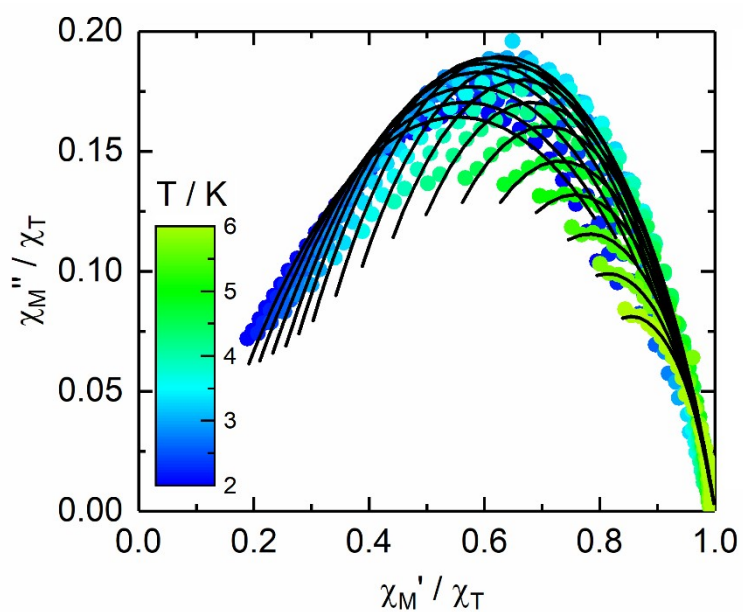


**Figure S20.** Normalized Argand plot for **3-Dy** in the temperature range of 2-6 K at 1000 Oe. Full black lines are the best fits obtained from the extended Debye equation.

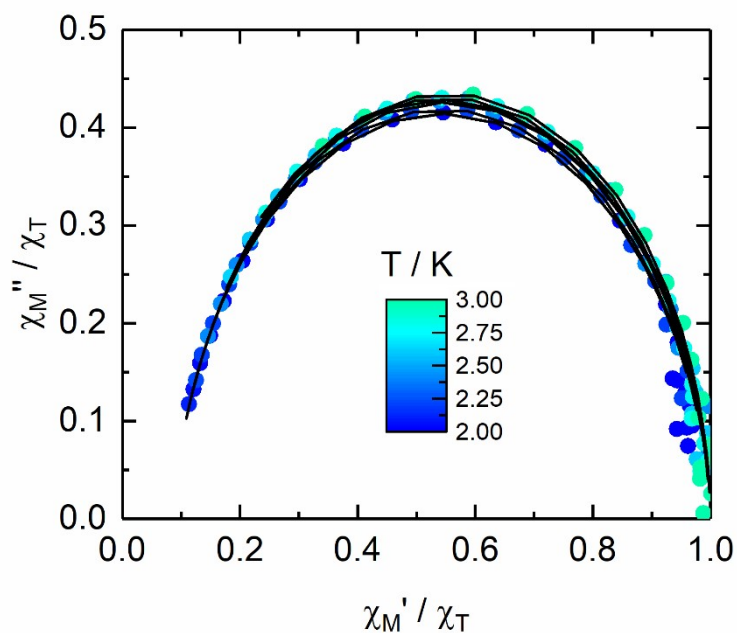


**Figure S21.** Normalized Argand plot for **4-Yb** in the temperature range of 2-3 K at 1000 Oe. Full black lines are the best fits obtained from the extended Debye equation.

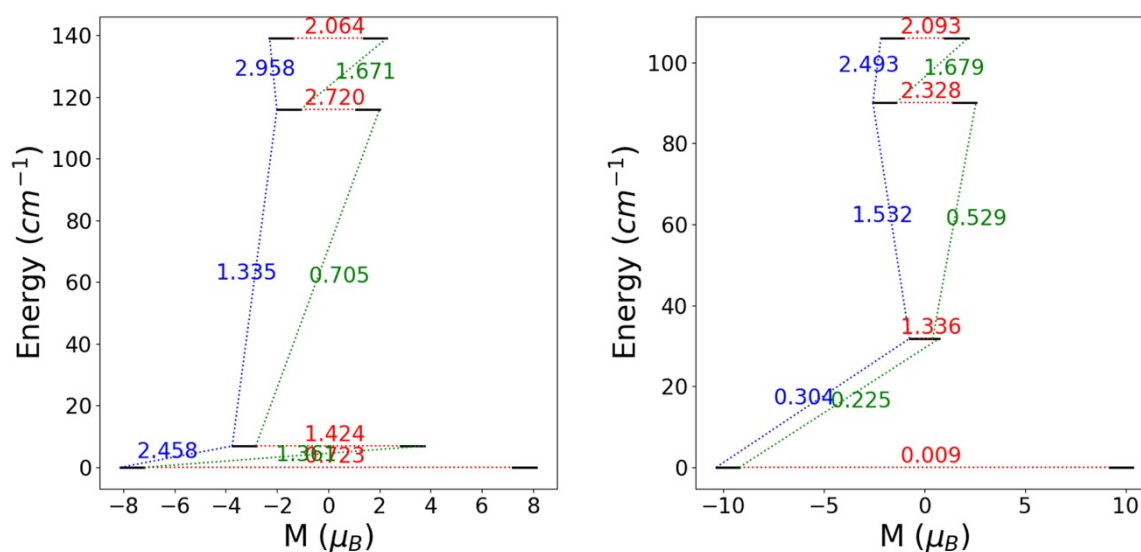


**Figure S22.** Energies (in  $\text{cm}^{-1}$ ) and projected  $\mu_z$  (in  $\mu_B$ ) values along the ground magnetic axis for **1-Dy** (left) and **3-Dy** (right). Black lines represent the four lowest Kramer doublets of each complex. The values of the magnetic (i.e. isotropic Zeeman) transition moments between the states are given for comparison. The values in red correspond to QTM (for the GS) and TA-QTM (for the ES) mechanisms of the magnetization relaxation, whereas blue and green values correspond to Orbach mechanisms.

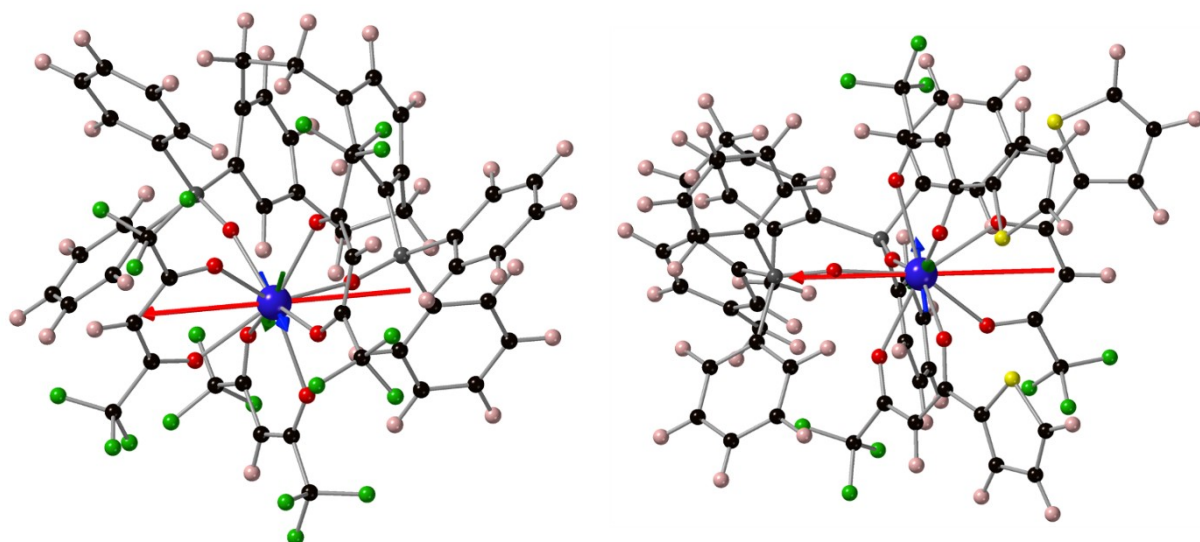


**Figure S23.** Representation of the orientation of the computed local ground state magnetic anisotropy axes for **1-Dy** (left) and **3-Dy** (right).

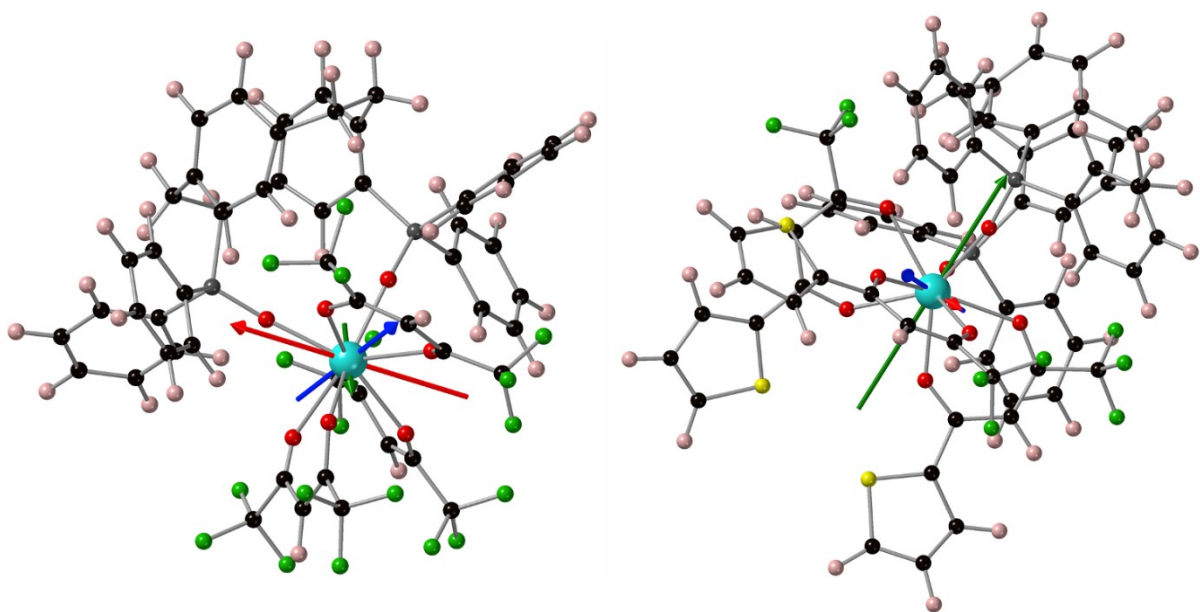


**Figure S24.** Representation of the orientation of the computed local ground state magnetic anisotropy axes for **2-Yb** (left) and **4-Yb** (right).

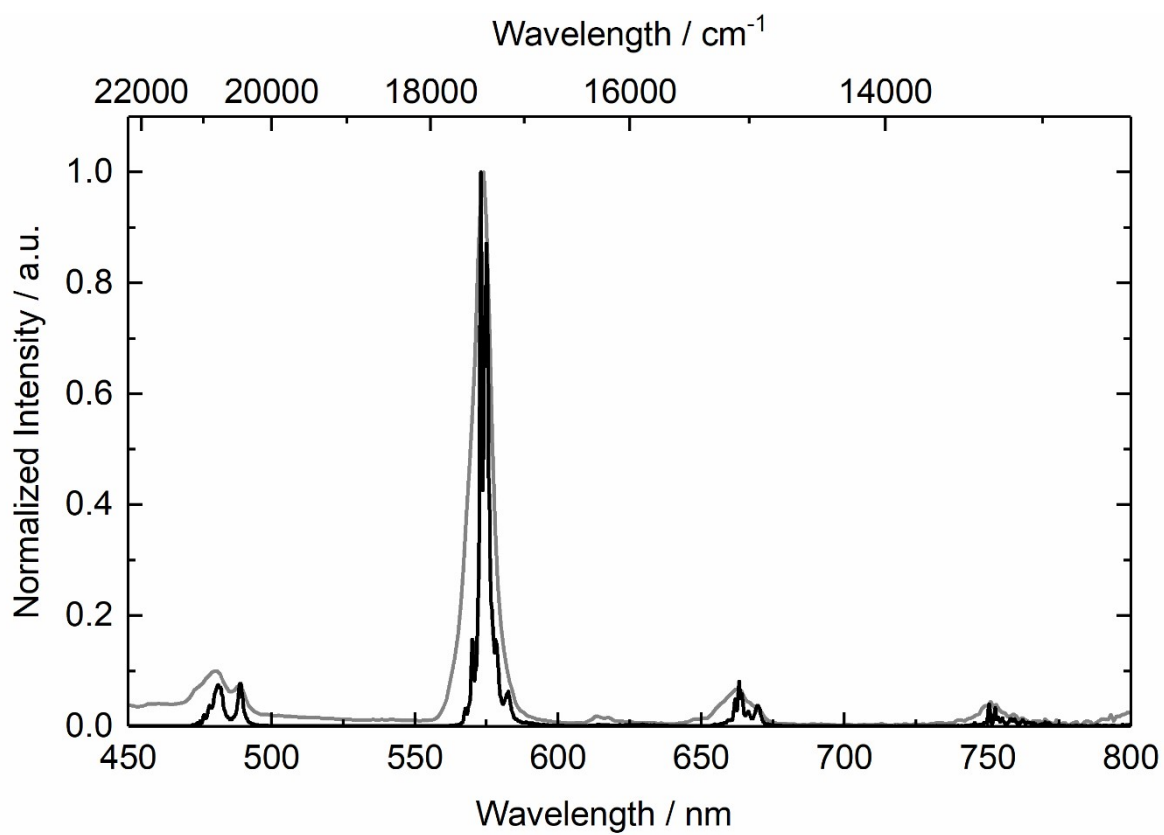


**Figure S25.** Room (grey line) and low (black line) temperature (77 K) emission in solid-state under irradiation at  $\lambda_{\text{exc}}=340$  nm for **1-Dy**.

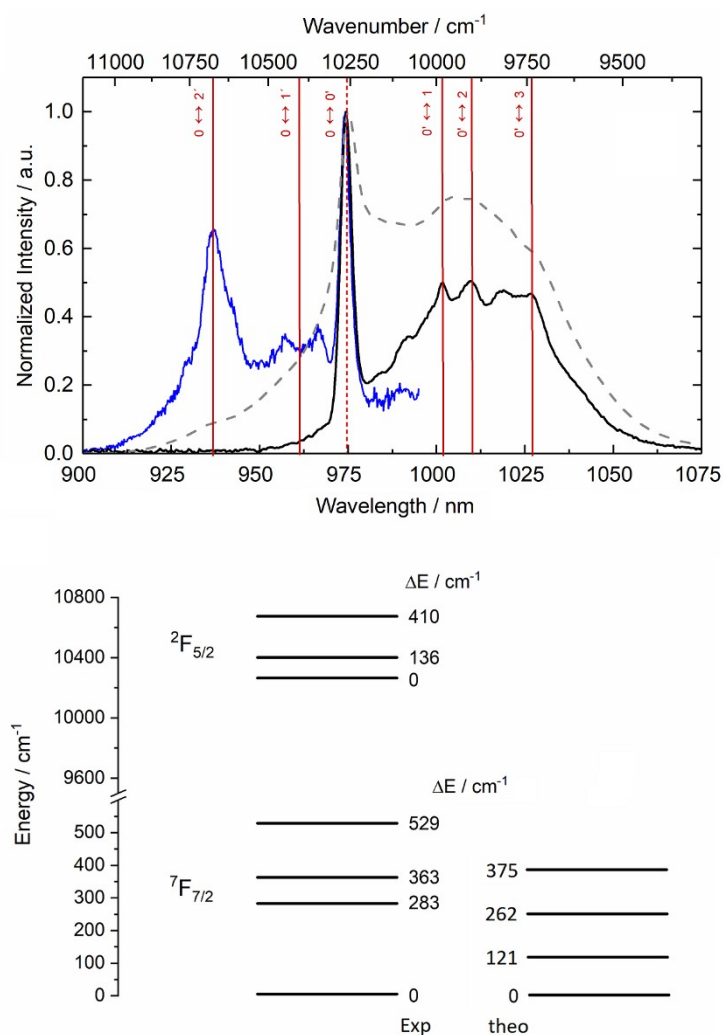


**Figure S26.** Room (dashed grey line) and low (full black line) temperature (77 K) solid state emission spectra for **4-Yb** under irradiation at  $\lambda_{\text{exc}}=340$  nm and their corresponding excitation spectra (full blue line) obtained by detection at 1025 nm. The vertical red sticks represent the experimental energy splitting of the <sup>2</sup>F<sub>5/2</sub> and <sup>2</sup>F<sub>7/2</sub> levels with the dashed vertical sticks indicating the zero-phonon line. The corresponding energy diagrams of the ground and first excited state splitting for the three compounds are depicted on the bottom part of the corresponding spectra.

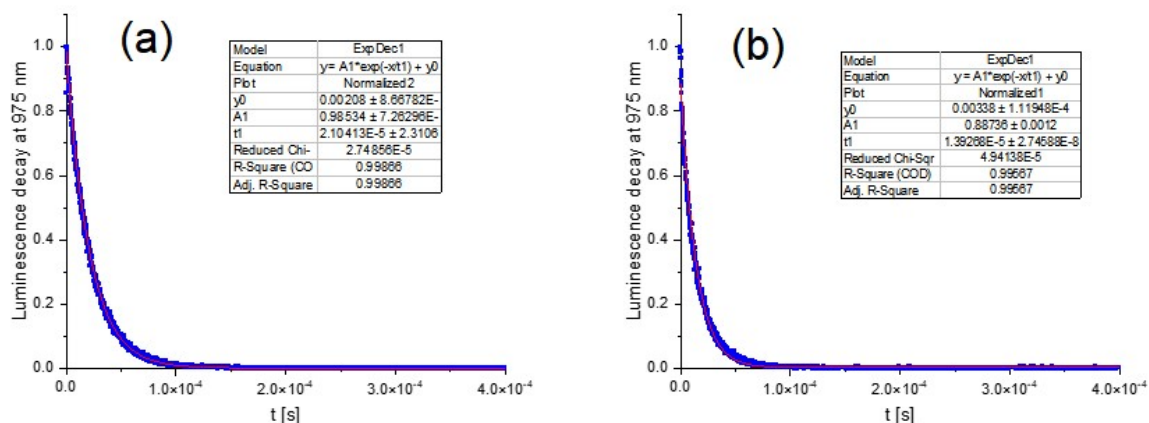


**Figure S27.** Emission lifetime decays (blue dots) and mono-exponential fit curves (red line) for **2-Yb** (a) and **4-Yb** (b) in  $\text{CH}_2\text{Cl}_2$  solution excited at 340 nm.

**Table S9.** Computed energies levels (the ground state is set at zero), component values of the Lande factor  $g$  and wavefunction composition for each  $M_J$  state of the ground-state multiplet for the Dy center in **1-Dy**. Calculations carried out at the CASSCF level.

	$E$ ( $\text{cm}^{-1}$ )	$g_x$	$g_y$	$g_z$	WFT
1	0.0	0.4	3.9	15.3	$0.63 \pm 15/2\rangle + 0.11 \pm 13/2\rangle$
2	6.9	0.4	3.6	14.8	$0.26 \pm 1/2\rangle + 0.23 \pm 3/2\rangle + 0.19 \pm 5/2\rangle + 0.17 \pm 7/2\rangle$
3	115.9	11.0	7.4	1.6	$0.26 \pm 7/2\rangle + 0.24 \pm 5/2\rangle + 0.21 \pm 3/2\rangle + 0.21 \pm 1/2\rangle$
4	139.1	2.3	4.0	9.8	$0.21 \pm 1/2\rangle + 0.21 \pm 3/2\rangle + 0.17 \pm 5/2\rangle + 0.14 \pm 7/2\rangle$
5	167.9	1.9	5.1	12.0	$0.40 \pm 11/2\rangle + 0.26 \pm 9/2\rangle$
6	206.6	1.9	3.0	13.7	$0.26 \pm 3/2\rangle + 0.24 \pm 5/2\rangle + 0.20 \pm 7/2\rangle + 0.14 \pm 9/2\rangle$
7	225.5	0.6	1.4	17.5	$0.34 \pm 7/2\rangle + 0.29 \pm 5/2\rangle + 0.18 \pm 3/2\rangle + 0.12 \pm 1/2\rangle$
8	313.1	0.0	0.1	19.4	$0.42 \pm 13/2\rangle + 0.35 \pm 11/2\rangle + 0.11 \pm 9/2\rangle$

**Table S10.** Computed energies levels (the ground state is set at zero), component values of the Lande factor  $g$  and wavefunction composition for each  $M_J$  state of the ground-state multiplet for the Dy center in **3-Dy**. Calculations carried out at the CASSCF level.

	$E$ (cm <sup>-1</sup> )	$g_x$	$g_y$	$g_z$	WFT
1	0.0	0.0	0.0	19.5	$0.95 \pm 15/2\rangle$
2	31.8	0.1	0.3	18.9	$0.54 \pm 1/2\rangle + 0.33 \pm 3/2\rangle + 0.11 \pm 5/2\rangle$
3	90.1	1.8	4.5	13.7	$0.38 \pm 3/2\rangle + 0.23 \pm 1/2\rangle + 0.13 \pm 5/2\rangle + 0.12 \pm 9/2\rangle$
4	106.0	0.8	5.0	10.8	$0.46 \pm 5/2\rangle + 0.30 \pm 7/2\rangle$
5	132.7	9.9	6.4	2.4	$0.31 \pm 13/2\rangle + 0.24 \pm 7/2\rangle + 0.21 \pm 5/2\rangle + 0.10 \pm 9/2\rangle$
6	150.6	1.9	3.9	13.6	$0.21 \pm 9/2\rangle + 0.20 \pm 13/2\rangle + 0.20 \pm 7/2\rangle + 0.15 \pm 1/2\rangle$
7	255.0	0.1	0.2	19.2	$0.40 \pm 11/2\rangle + 0.29 \pm 9/2\rangle + 0.19 \pm 13/2\rangle$
8	279.9	0.0	0.1	19.6	$0.35 \pm 11/2\rangle + 0.24 \pm 9/2\rangle + 0.21 \pm 13/2\rangle + 0.13 \pm 7/2\rangle$

**Table S11.** Computed energies levels (the ground state is set at zero), component values of the Lande factor  $g$  and wavefunction composition for each  $M_J$  state of the ground-state multiplet for the Yb center in **2-Yb**. Calculations carried out at both CASSCF and CASPT2 level.

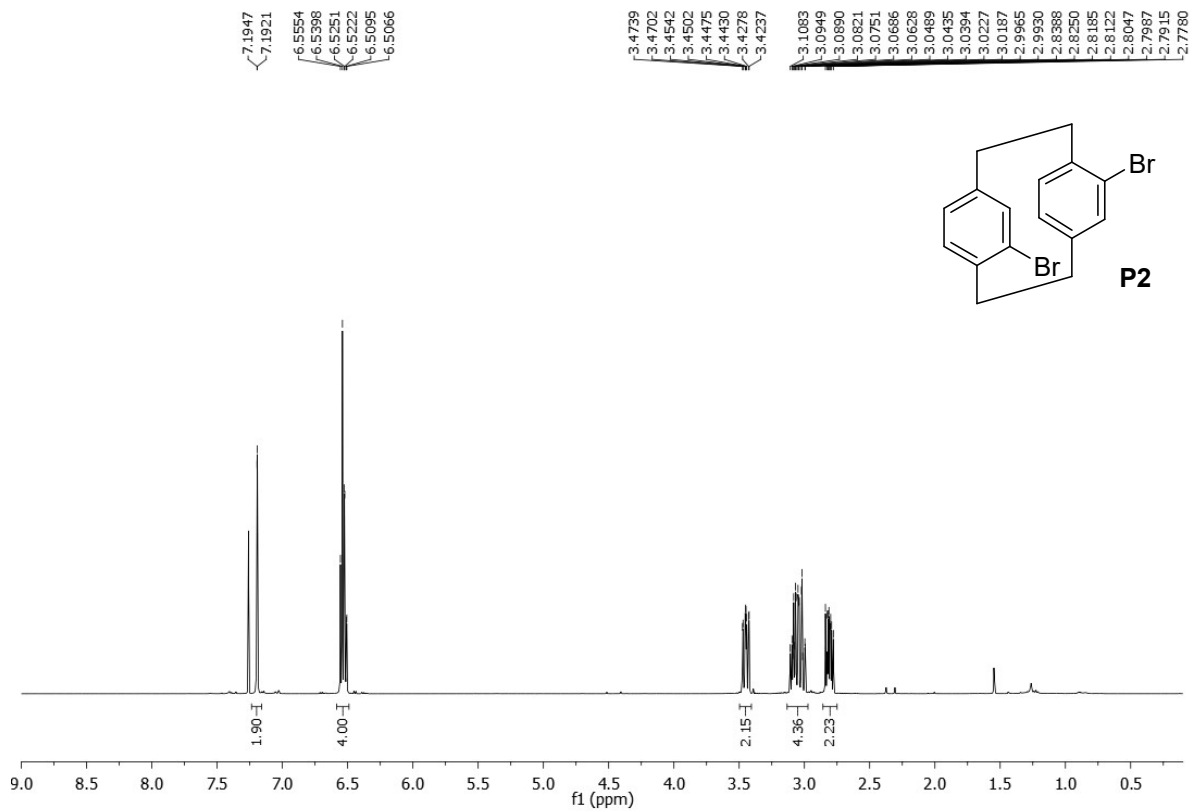
	$E$ (cm <sup>-1</sup> )	$g_x$	$g_y$	$g_z$	WFT
CASSCF					
1	0.0	4.9	3.2	1.2	$0.59 \pm 1/2\rangle + 0.26 \pm 3/2\rangle + 0.11 \pm 5/2\rangle$
2	151.5	0.7	1.4	6.4	$0.38 \pm 3/2\rangle + 0.37 \pm 1/2\rangle + 0.19 \pm 5/2\rangle$
3	183.1	1.1	2.5	4.5	$0.53 \pm 5/2\rangle + 0.33 \pm 3/2\rangle + 0.11 \pm 7/2\rangle$
4	432.6	0.2	0.5	7.6	$0.79 \pm 7/2\rangle + 0.17 \pm 5/2\rangle$
CASPT2					
1	0.0	1.2	3.0	4.9	$0.40 \pm 5/2\rangle + 0.27 \pm 7/2\rangle + 0.26 \pm 3/2\rangle$
2	217.2	3.5	3.3	1.4	$0.32 \pm 3/2\rangle + 0.32 \pm 7/2\rangle + 0.26 \pm 1/2\rangle$
3	255.8	0.1	1.9	4.8	$0.38 \pm 7/2\rangle + 0.37 \pm 5/2\rangle + 0.19 \pm 1/2\rangle$
4	543.1	0.2	0.6	7.4	$0.48 \pm 1/2\rangle + 0.35 \pm 3/2\rangle + 0.14 \pm 5/2\rangle$

**Table S12.** Computed energies levels (the ground state is set at zero), component values of the Lande factor  $g$  and wavefunction composition for each  $M_J$  state of the ground-state multiplet for the Yb center in **4-Yb**. Calculations carried out at both CASSCF and CASPT2 level.

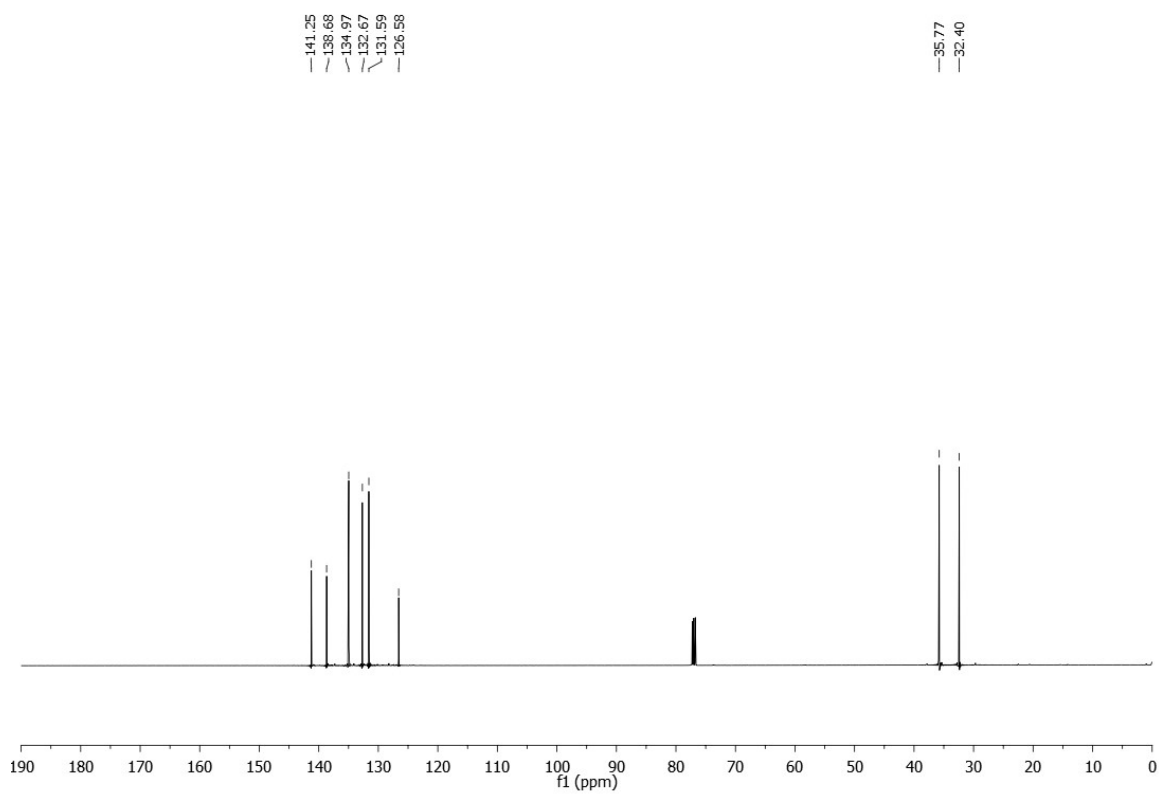
	$E$ (cm <sup>-1</sup> )	$g_x$	$g_y$	$g_z$	WFT
CASSCF					
1	0.0	0.5	2.7	5.0	$0.39 \pm 7/2\rangle + 0.29 \pm 5/2\rangle + 0.19 \pm 3/2\rangle + 0.13 \pm 1/2\rangle$
2	84.7	1.2	1.8	4.7	$0.45 \pm 1/2\rangle + 0.34 \pm 7/2\rangle + 0.18 \pm 3/2\rangle$
3	178.3	4.7	3.0	1.0	$0.34 \pm 3/2\rangle + 0.30 \pm 5/2\rangle + 0.19 \pm 1/2\rangle + 0.17 \pm 7/2\rangle$
4	240.8	0.7	1.4	5.7	$0.39 \pm 5/2\rangle + 0.28 \pm 3/2\rangle + 0.23 \pm 1/2\rangle + 0.10 \pm 7/2\rangle$
CASPT2					
1	0.0	4.9	2.7	0.3	$0.50 \pm 3/2\rangle + 0.36 \pm 5/2\rangle + 0.10 \pm 1/2\rangle$
2	120.5	1.3	2.0	4.4	$0.46 \pm 1/2\rangle + 0.40 \pm 7/2\rangle + 0.13 \pm 3/2\rangle$
3	262.1	4.0	3.2	0.6	$0.31 \pm 7/2\rangle + 0.31 \pm 5/2\rangle + 0.22 \pm 3/2\rangle + 0.16 \pm 1/2\rangle$
4	374.5	0.7	1.5	5.5	$0.32 \pm 5/2\rangle + 0.29 \pm 1/2\rangle + 0.25 \pm 7/2\rangle + 0.15 \pm 3/2\rangle$

4,12-Dibromo[2.2]paracyclophane (**P2**)

$^1\text{H}$  NMR ( $\text{CDCl}_3$ , 500 MHz)

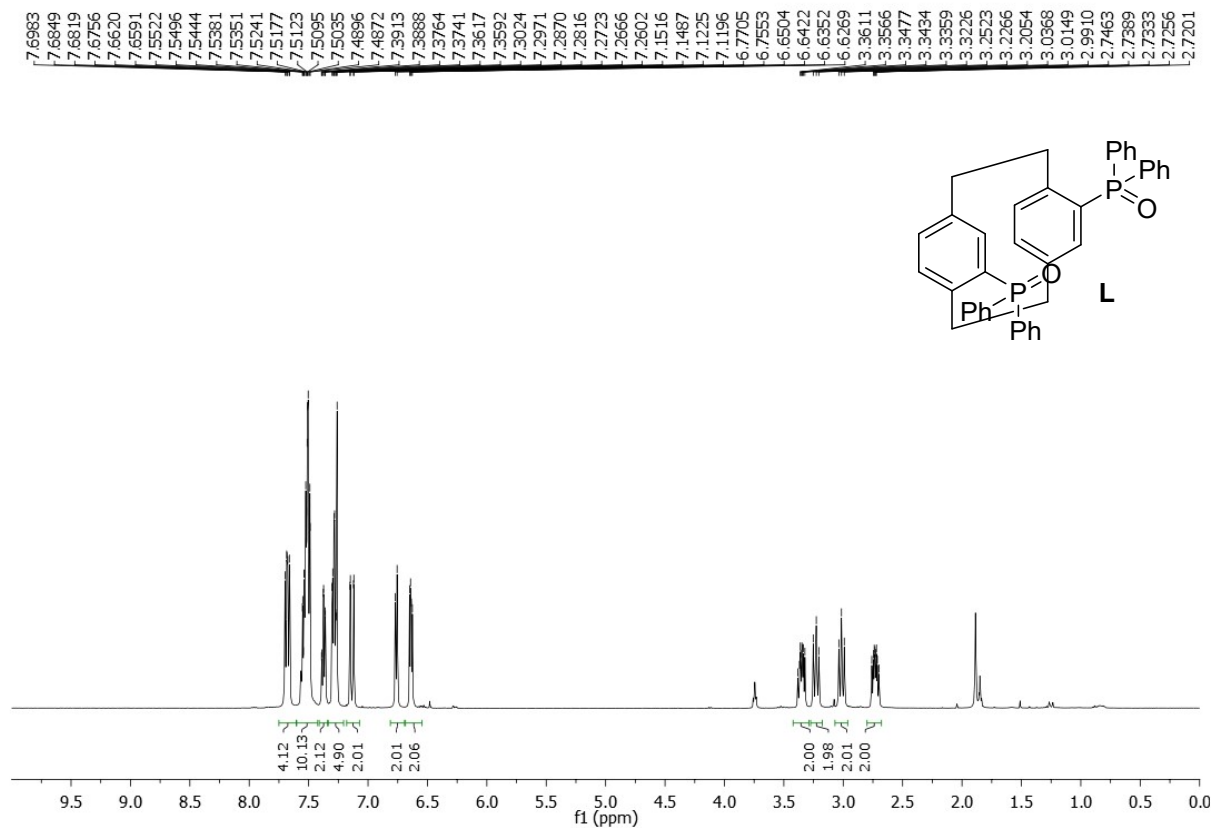


$^{13}\text{C}\{^1\text{H}\}$  NMR ( $\text{CDCl}_3$ , 125 MHz)

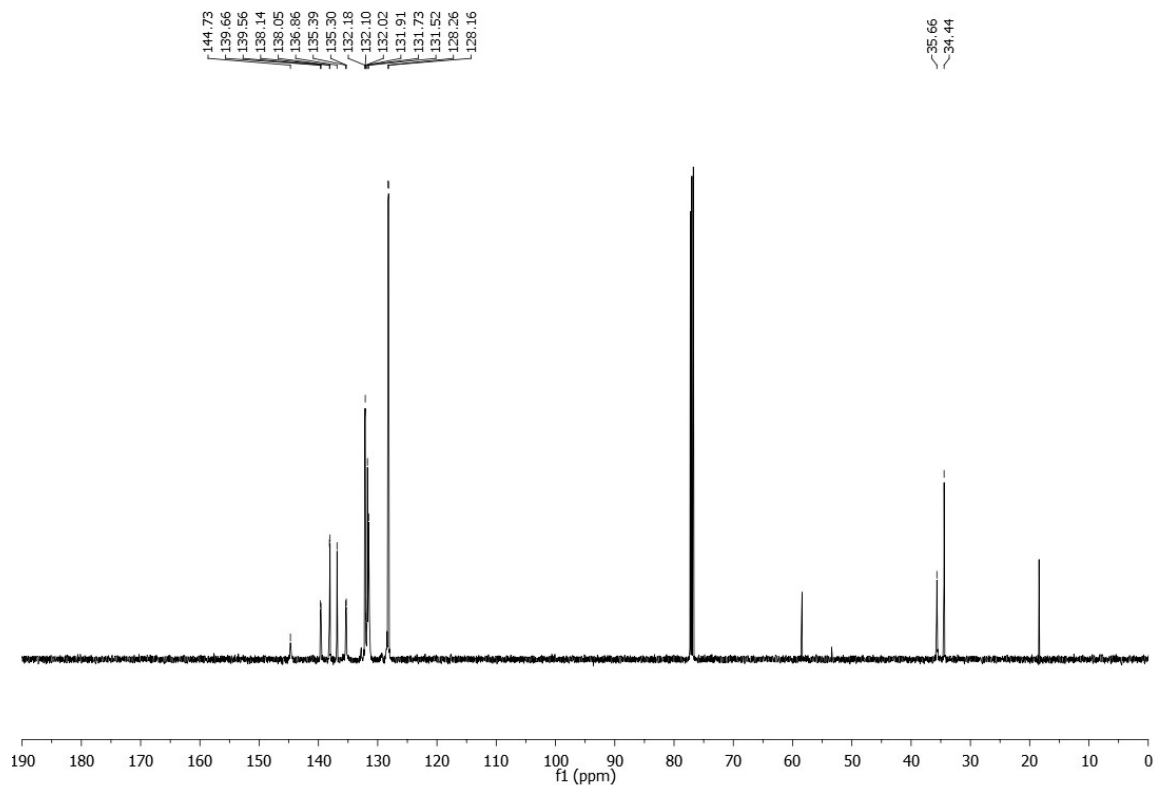


1,4(1,4)-Dibenzenacyclohexaphane-1<sup>2</sup>,4<sup>3</sup>-diylbis(diphenylphosphine oxide) (**L**)

<sup>1</sup>H NMR (CDCl<sub>3</sub>, 500 MHz)



<sup>13</sup>C{<sup>1</sup>H} NMR (CDCl<sub>3</sub>, 125 MHz)



**$^{31}\text{P}$  NMR ( $\text{CDCl}_3$ , 202 MHz)**

—24.66

